Received: 27 March 2024 | Accepted: 21 December 2024

DOI: 10.1097/HEP.0000000000001244

ORIGINAL ARTICLE

OPEN

Short-term starvation boosts anti-PD-L1 therapy by reshaping tumor-associated macrophages in hepatocellular carcinoma

Kun Cheng[1,2,3] | **Ning Cai**[1,2,3] | **Xing Yang**[4] | **Danfeng Li**[1,2,3] | **Jinghan Zhu**[1,2,3] | **Hui Yuan Yang**[1,2,3] | **Sha Liu**[1,2,3] | **Deng Ning**[1,2,5] | **Huifang Liang**[1,2,3] | **Jianping Zhao**[1,2,3] | **Zhanguo Zhang**[1,2,3] | **Wanguang Zhang**[1,2,3,6]

[1]Hepatic Surgery Centre, Tongji Hospital, Tongji Medical College, Huazhong University of Science and Technology, Wuhan, Hubei, China

[2]Hubei Key Laboratory of Hepato-Pancreato-Biliary Diseases, Tongji Hospital, Tongji Medical College, Huazhong University of Science and Technology, Wuhan, Hubei, China

[3]Clinical Medicine Research Centre for Hepatic Surgery of Hubei Province, Tongji Hospital, Tongji Medical College, Huazhong University of Science and Technology, Wuhan, Hubei, China

[4]Department of Internal Medicine and Institute of Hypertension, Tongji Hospital, Tongji Medical College, Huazhong University of Science and Technology, Wuhan, Hubei

[5]Department of Hepatobiliary Surgery, Union Hospital, Tongji Medical College, Huazhong University of Science and Technology, Wuhan, Hubei, China

[6]Key Laboratory of Organ Transplantation, Ministry of Education; NHC Key Laboratory of Organ Transplantation; Key Laboratory of Organ Transplantation, Chinese Academy of Medical Sciences, Wuhan, China.

Correspondence
Huifang, Liang, Tongji Hospital, Huazhong University of Science and Technology, Hepatic Surgery Centre, 1095 Jiefang Avenue, Wuhan, Hubei Province 430030, China.
Email: lianghuifang1997@126.com

Jianping Zhao, Tongji Hospital of Tongji Medical College of Huazhong, University of Science and Technology, Hepatic Surgery Centerd, 1095 Jiefang Avenue, Wuhan, Hubei Province, 430030, China.
Email: jpzhao@hust.edu.cn

Zhanguo Zhang, Tongji Hospital, Tongji Medical College, Huazhong, University of Science and Technology, Hepatic Surgery Center, 1095 Jiefang Avenue, Wuhan, Hubei Province, 430030, China.
Email: zhanguo_tjh@hust.edu.cn

Abstract

Background and Aims: Immune checkpoint inhibitors have revolutionized systemic HCC treatment. Nevertheless, numerous patients are refractory to immune checkpoint inhibitor therapy. It is currently unknown whether diet therapies such as short-term starvation (STS) combined with immune checkpoint inhibitors can be used to treat HCC. This study aimed to investigate whether STS could sensitize HCC tumors to immunotherapy.

Approach and Results: STS was found to attenuate tumor progression by inducing tumor-associated macrophages (TAMs) to switch to an antitumoral phenotype, enhancing phagocytosis of tumor cells, and stimulating subsequent antitumor immunity of $CD8^+$ T cells as demonstrated in 3 HCC mouse models, NCG mice, and Rag2-KO mice. Furthermore, STS combined with

Abbreviations: aTAMs, antitumoral TAMs; BMDMs, bone marrow–derived macrophages; ER, energy restriction; exoPD-L1, exosomal PD-L1; FBP1, fructose diphosphatase 1; FMD, fasting-mimic diet; ICIs, immune checkpoint inhibitors; $GZMB^+$, Granzyme B^+; IFNγ, interferon-γ; LAG-3, lymphocyte Activation Gene-3; MDSCs, myeloid-derived suppressor cells; ND, normal diet; PD-1, programmed cell death-1; PD-L1, programmed cell death ligand 1; pTAMs, protumoral TAMs; SCR, severe calorie restriction; STS, short-term starvation; TAMs, tumor-associated macrophages; T_{CM}, central memory T cell; T_{RM}, tissue-resident memory T cells; TIM-3, T-cell immunoglobulin and mucin domain-3; TME, tumor microenvironment.

Kun Cheng, Ning Cai, and Xing Yang contributed equally to this work.

Supplemental Digital Content is available for this article. Direct URL citations are provided in the HTML and PDF versions of this article on the journal's website, www.hepjournal.com.

Wanguang Zhang, Hepatic Surgery Centre, Tongji Hospital, Tongji, Medical College, Huazhong University of Science and Technology, 1095 Jiefang Avenue, Wuhan, Hubei Province, 430030, China.
Email: wgzhang@tjh.tjmu.edu.cn

anti-programmed cell death 1/ligand 1 (anti-PD-1/L1) suppressed tumor progression, while the efficacy of PD-L1 was improved when combined with STS. Mechanistically, TAM-derived exosomal PD-L1 (exoPD-L1) impairs the efficacy of anti-PD-1/L1. STS attenuates exoPD-L1 secretion from TAM by regulating the fructose diphosphatase 1 (FBP1) /Akt/Rab27a axis. Modulating FBP1/Akt/Rab27a axis potentiates the anti-PD-L1 response using 2 liposomal delivery systems and macrophage adoptive transfer.

Conclusions: This study describes the immunomodulatory effects of STS and provides a rationale for its application as an adjuvant in HCC immunotherapy.

Keywords: $CD8^+$ T cell, diet therapies, exosome, immunotherapy, tumor-associated macrophage

INTRODUCTION

An altered tumor microenvironment (TME) induced by dietary intervention has been described as a critical cancer hallmark.[1] Emerging evidence indicates that dietary modifications such as cyclic starvation, calorie-restricted diets, ketogenic diet, and low-protein diets represent promising strategies for suppressing tumor growth.[1–5] Energy restriction (ER) regimens represented by short-term starvation (STS) and fasting-mimic diet (FMD), are currently the most popular therapeutic diets used in clinical practice.[6] Fasting increases $CD8^+$ T-cell infiltration and reduces immunosuppressive regulatory T cells or myeloid-derived suppressor cells (MDSCs).[7–9] Additionally, fasting affects the monocyte pool.[10] Overall, these studies suggest that starvation regimens could remodel the immune system.[2,7,11–13] Moreover, in a clinical trial, FMD was found to be safe and boost antitumor immunity.[8]

Most studies on dietary regulation in cancer have focused on lymphocytes.[2,9] Tumor-associated macrophages (TAMs) are among the most abundant immune cells in the TME.[14] The reprogramming of protumoral TAMs (pTAMs) to antitumoral TAMs (aTAMs) has become one of the most favored immunotherapy strategies.[15] Nevertheless, the effects of fasting on the metabolism and function of macrophages remain unclear. Therefore, reprogramming TAMs through dietary regulation has great potential for improving the effectiveness of immunotherapy.

HCC is the fifth most common cancer and one of the deadliest cancers worldwide, with an extremely poor prognosis.[16] Previous studies have investigated the role of dietary restriction in sensitizing cancer cells to chemotherapeutics, radiotherapy, endocrine therapies, and multitarget kinase inhibitors.[3,9,17–19] Although immunotherapy is the primary treatment option for patients with HCC, many remain refractory to it. Only 15%–20% of patients benefit from immune checkpoint inhibitors (ICI) therapy.[20,21] The absence of immune checkpoints and the inability of antibodies to bind to targets effectively are primary reasons for ICI resistance. Inflammatory cells, including TAMs, express higher levels of immune checkpoint proteins such as programmed cell death ligand 1 (PD-L1) than tumor cells.[22,23] Moreover, the PD-L1 expression pattern on the surface of tumor cells is short-lived and dependent on Interferon-γ (IFN-γ).[24] Even when PD-L1 is removed from the surface of tumor cells, its expression on immune cells is maintained.[25] Blocking $PD\text{-}L1^+$ myeloid cells is indispensable for enhancing antitumor immune responses.[23,26,27] In addition, PD-L1 is released from cells into the extracellular space to form free PD-L1, including exosomal PD-L1 (exoPD-L1) and soluble (extracellular) PD-L1.[28] Compared to soluble (extracellular) PD-L, exoPD-L1 is not easily degraded and can induce T-cell dysfunction.[29,30] Furthermore, knockout of key molecules that regulate exosome secretion alleviates ICIs resistance.[30] Therefore, suppressing exoPD-L1 release from TAMs may be an effective strategy for eradicating liver malignancies.

Therefore, we aimed to explore the effects of dietary therapy on HCC immunotherapy and prognosis. Revealing the regulatory mechanisms of STS in the TME will increase our understanding of immune tolerance in HCC. In addition, we aimed to determine whether STS could be used as an additive or synergistic therapy for ICIs to improve the clinical translational significance of dietary therapy.

METHODS

Animals and tumor treatments

C57BL/6J mice, NCG mice, and GFP mice were purchased from GemPharmatech (Nanjing, China) and

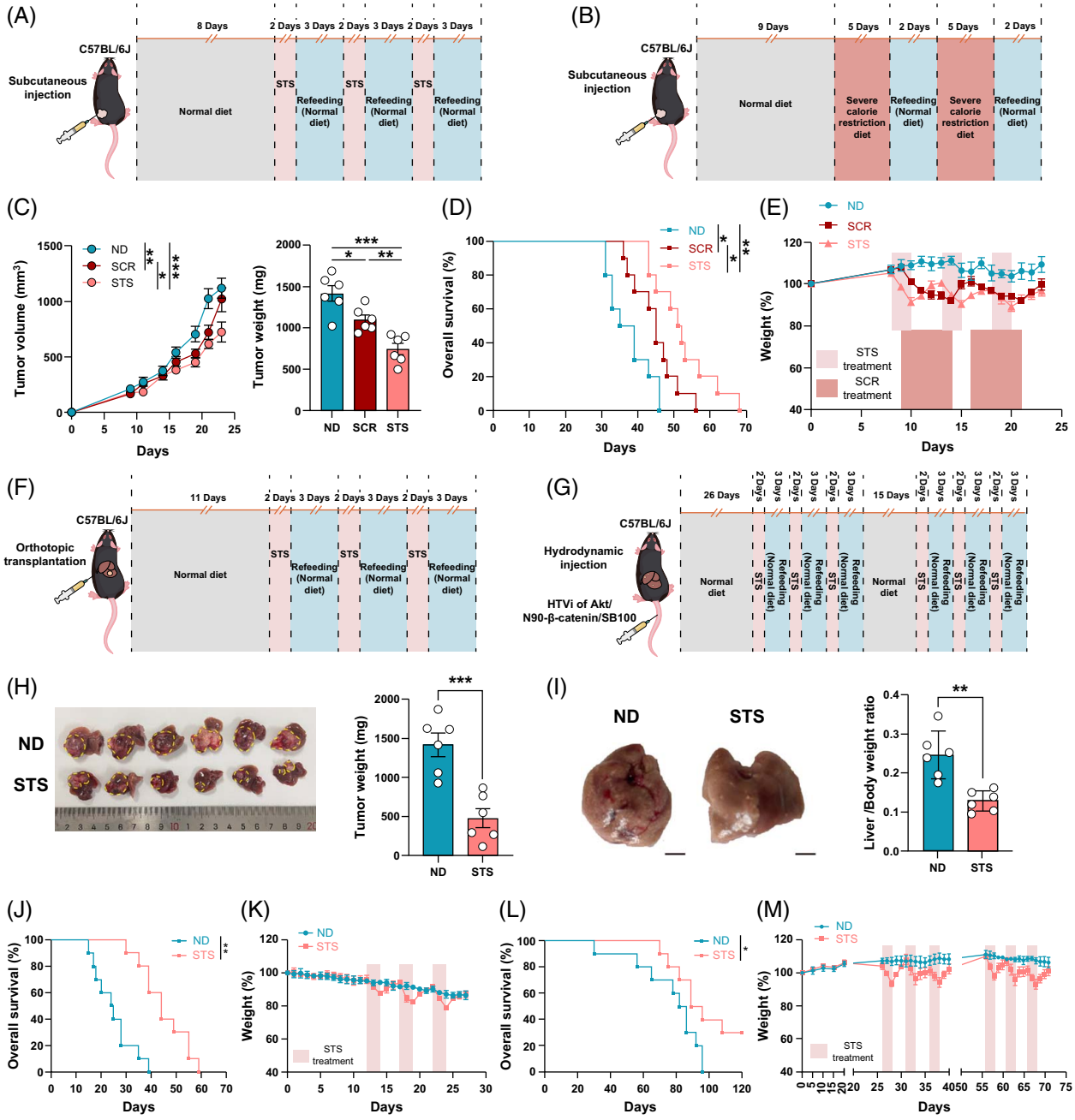

FIGURE 1 STS suppresses the growth of multiple HCC types. (A, B) Schematic diagram of the experimental approach of the STS and SCR regimen (described in Methods section). (C) Tumor size or weight analysis over time (n = 6 mice per group). (D) Survival curve of the mice from the ND, SCR, and STS groups (n = 10 mice per group). (E) Daily body weight change during the experimental period, expressed as the percentage of body weight relative to pre-experiment levels (n = 6 mice per group). (F, G) Schematic diagram of the experimental approach of STS in the orthotopic and hydrodynamic HCC models. (H, I) Gross tumor images and weight statistics in the orthotopic and hydrodynamic HCC models (n = 6 mice per group), scale bar = 5 mm. (J) Survival curve of the mice from the orthotopic HCC model (n = 10 mice per group). (K) Daily body weight of the mice from the orthotopic HCC model (n = 6 mice per group). (L) Survival curve of the mice from the hydrodynamic HCC model (n = 10 mice per group). (M) Daily body weight of mice from the hydrodynamic HCC model (n = 6 mice per group). Error bars represent the mean ± SEM. Statistical analyses were performed using Student *t* test, one-way ANOVA, and two-way ANOVA with Tukey multiple comparisons test, and Log-rank test, $^{*}p < 0.05$, $^{**}p < 0.01$, $^{***}p < 0.001$. Abbreviations: ND, normal diet; SCR, severe calorie restriction; STS, short-term starvation.

BEIANTE (Nanjing, China). Rag2-KO ($Rag2^{-/-}$) mice and OT-1 mice were purchased from Cyagen Biosciences Inc. These animals were housed in a specific pathogen-free environment. All animal experiments were performed following the internationally accepted principles and Guidelines for the Care and Use of Laboratory Animals at Huazhong University of Science and Technology. The experiment protocols were approved by the Institutional Animal Ethical Committee of the Huazhong University of Science and Technology.

For the subcutaneous HCC model, Hepa1-6 cells (2×10^6) were subcutaneously injected into the flanks of C57BL/6J mice, Rag2-KO mice, and NCG mice. Mice underwent STS (days 8–10, 13–15, and 18–20). For the severe calorie restriction (SCR) regime, mice were fed a diet with 80% less energy for 5 days followed by 2 days of refeeding, 2 cycles (days 9–14 and days 16–21). Anti-PD-1 (BioXCell or GC42, TopAlliance Jiang su, China) or anti-PD-L1 (Durvalumab, IMFINZI) i.p. inoculation was performed on days 9, 14, and 19 (200 μg/per mouse). For the Orthotopic HCC model, Hepa1-6 cells (8×10^5) were injected orthotopically in the left lobe of the mouse liver. HCC tumors were allowed to grow for 11 days before treatment. Next, mice underwent complete food deprivation with free access to water for 3 cycles of 2 days (days 12–14, 17–19, and 22–24). Anti-PD-1 or anti-PD-L1 was administered by i.p. (intraperitoneally) injection on days 13, 18, and 23 (200 μg/per mouse). For the hydrodynamic HCC model, pT3-myr-Akt-HA and pT3-N90-beta-catenin were gifts from Xin Chen (Addgene plasmid #31789 and #31785), pCMV (CAT) T7-SB100 was a gift from Zsuzsanna Izsvak (Addgene plasmid #34879). Hydrodynamic injection has also been described.[31] Briefly, 3.75 μg pCMV (CAT) T7-SB100, 20 μg pT3-myr-Akt-HA, and pT3-N90-beta-catenin were suspended in PBS and subsequently injected into the lateral tail veins of male 6-week-old mice (0.1 mL/g body weight). Mice were treated with STS (first cycle: days 26–28, 31–33, and 36–38; second cycle: days 56–58, 61–63, and 66–68).

Depletion of macrophages was performed by i.p. injection of Clophosome-Clodronate liposomes or isotype (Control liposome), (F70101C-N, FormuMax). During the first injection, 1.4 mg was administered followed by 0.7 mg every 4 days for 4 cycles. Depletion of $CD8^+$ T cells was performed by i.p. injection of 200 μg anti-mouse CD8α (BE0004-1, clone 53-6.7, BioXCell) every 4 days for 4 cycles. All depletion assays were performed in 6-week-old C57BL/6J mice.

Statistical analyses

All statistical analyses and graph generation were performed using GraphPad Prism 9.0. Flow cytometry data and graphs were analyzed using Flow jo V10 and CytExpert. Student *t* test (2 groups) or One-way ANOVA with Tukey multiple comparisons test (more than 2 groups) was performed to analyze data between 2 experimental groups. Two-way ANOVA was performed for tumor growth analysis. Kaplan-Meier and log-rank analyses were applied to evaluate survival between different groups. The data are presented as the mean ± SEM. Statistical significance was shown as $^*p<0.05$, $^{**}p<0.01$, and $^{***}p<0.001$.

RESULTS

STS inhibits HCC progression in subcutaneous, orthotopic, and hydrodynamic HCC mouse models

Recently, short-term ER therapy has been shown to inhibit tumor progression in several cancer types.[2,11,19,32] However, the effects of ER on gastrointestinal cancers, such as HCC remain unclear. Therefore, we tested the response to STS or SCR in the subcutaneous HCC model (Figures 1A, B). The STS regimen was adapted from a previously reported strategy.[2] SCR was achieved through intermittent periods of dietary restriction while allowing access to water ad libitum, similar to the FMD regimen.[7] STS showed greater efficacy in suppressing tumor growth and prolonging survival (Figures 1C, D; Supplemental Figures S1A, B, http://links.lww.com/HEP/J715). Weight loss occurred after each fasting session; however, the weight was regained with refeeding. Furthermore, the reduction in tumor growth was not caused by excessive weight loss (> 20% of the body weight) (Figure 1E).

We further tested STS in the orthotopic and hydrodynamic HCC mouse models (Figures 1F, G). Given that the hydrodynamic HCC model required a longer period for tumor formation, we administered three additional STS cycles (Figure 1G). STS consistently reduced tumor size in both HCC models (Figures 1H, I; Supplemental Figures S1C, D, http://links.lww.com/HEP/J715). The survival time after STS treatment was longer, indicating that the tumor reduction effect of STS was long-lasting (Figure 1J, L). STS allowed the remaining tumor-bearing mice to survive for a prolonged period in the hydrodynamic HCC model. Additionally, the STS diet did not cause significant cachexia (Figures 1K, M; Supplemental Figures S2A, B, http://links.lww.com/HEP/J715). Moreover, STS did not have noticeable pathological effects on the heart, spleen, lungs, and kidneys of mice in any of the 3 models (Supplemental Figures S2C–E, http://links.lww.com/HEP/J715).

Overall, the STS regimen was more effective in inhibiting tumor progression compared to SCR, functioning as a short-term treatment that provides safe, stable, and long-lasting effects in HCC-bearing mice.

STS reprograms the HCC immune microenvironment and reorganizes the immune cell pool

To determine whether STS causes HCC regression by directly inhibiting tumor cell growth or modulating the immune system, we cultured Hepa1-6 cells under high-nutrient or low-nutrient conditions to mimic a normal diet (ND) and STS regimens in vivo, respectively.[2] We engrafted tumor cells cultured under different nutrient

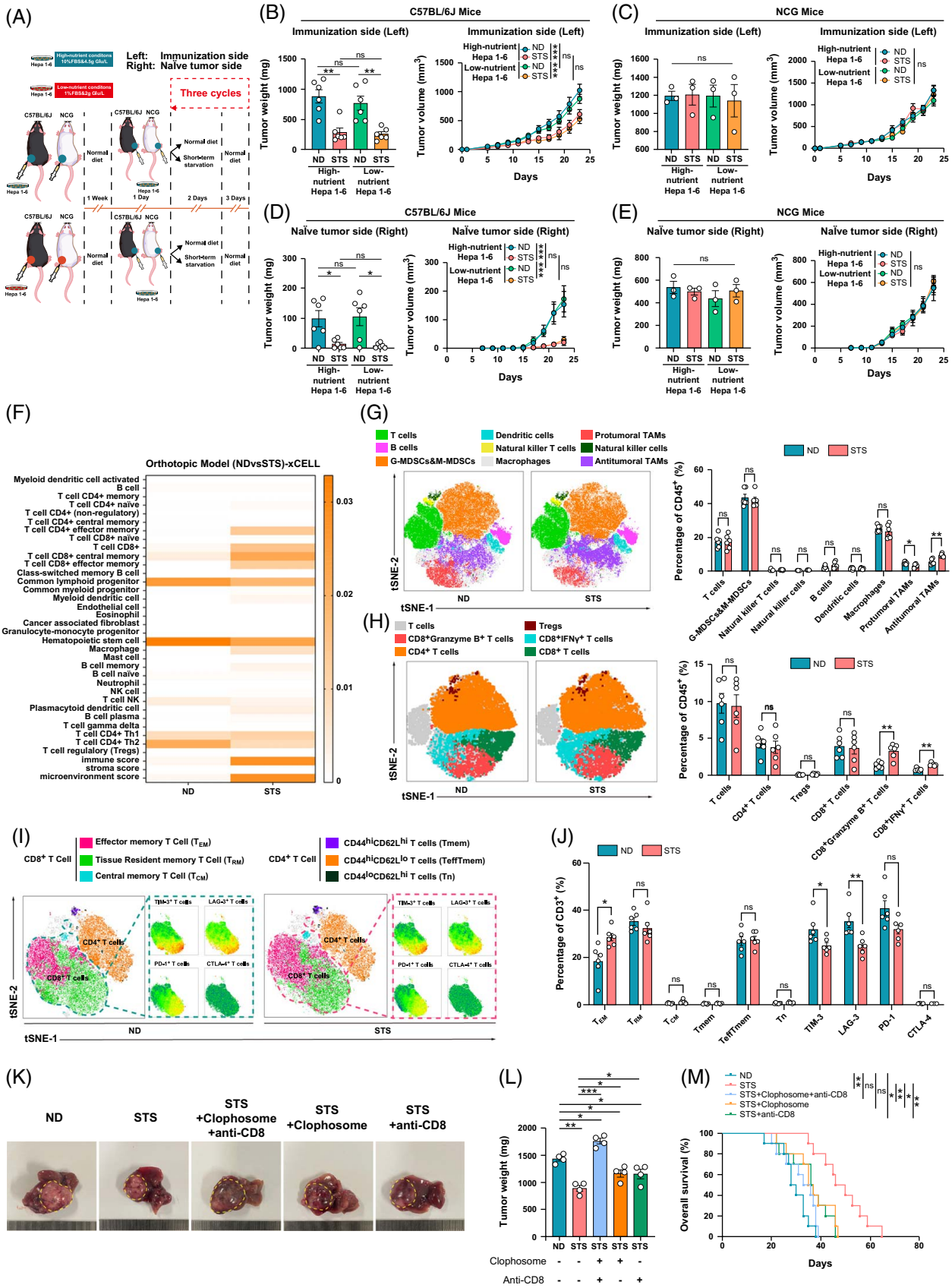

FIGURE 2 STS depends on systemic immunity and reconstructs the immune microenvironment. (A) Schematic diagram of the experimental approach. Hepa1-6 cells cultured under high-nutrient conditions (10% FBS and 4.5 g Glu/L) or low-nutrient conditions (1% FBS and 2 g Glu/L) were inoculated subcutaneously in the left flank (immunization side) of immunocompetent mice (C57BL/6J mice) or immunodeficient mice (NCG

mice). On the seventh day after the injection, Hepa1-6 cells cultured under high-nutrient conditions (10% FBS and 4.5 g Glu/L) were subcutaneously inoculated in the right flank (naive tumor side). (B) Tumor weight or size analysis of the immunization side of immunocompetent mice (n = 6 mice per group). (C) Tumor weight or size analysis of the immunization side of immunodeficient mice (n = 3 mice per group). (D) Tumor weight or size analysis of naive tumor side of immunocompetent mice (n = 6 mice per group). (E) Tumor weight or size analysis of naive tumor side of immunodeficient mice (n = 3 mice per group). (F) Immune infiltration was estimated using xCELL for expression profiles tested from RNA-seq data of the orthotopic HCC model (n = 3). (G) tSNE analysis using Flowjo was used to detect differences in the immunophenotypes of infiltrating immune cells detected by flow cytometry in the orthotopic HCC model from both the ND and STS groups. tSNE map derived from flow cytometric analysis indicating the populations of the infiltrating immune cells, including T cells ($CD45^+CD11b^-CD3^+$), G-MDSCs and M-MDSCs ($CD45^+CD11b^{hi}Gr1^{hi\ or\ mid}$), NKT cells ($CD45^+CD11b^-CD3^+NK1.1^+$), NK cells ($CD45^+CD11b^-CD3^-NK1.1^+$), B cells ($CD45^+CD11b^-CD3^-CD19^+$), Dendritic cells ($CD45^+CD11b^+Gr1^{lo}F4/80^-CD11c^+IA/IE^+$), Macrophages ($CD45^+CD11b^{hi}Gr1^{lo}F4/80^+$), pTAMs ($CD45^+CD11b^{hi}Gr1^{lo}F4/80^+CD86^{lo}CD206^{hi}$), aTAMs ($CD45^+CD11b^{hi}Gr1^{lo}F4/80^+CD86^{\ hi}\ CD206^{lo}$). Percentages of immune cell populations within $CD45^+$ cells are shown in the right panel (n = 6). (H) The functional state of the T cell subpopulation was analyzed by tSNE analysis and flow cytometric quantification; $CD4^+$ T cells ($CD3^+CD4^+CD8^-$), Tregs ($CD3^+CD4^+CD8^-\ CD25^+Foxp3^+$), $CD8^+$ T cells ($CD3^+CD4^-CD8^+$), Granzyme B^+ T cells ($CD8^+$ Granzyme B^+), $IFN\gamma^+$ T cells ($CD8^+\ IFN\gamma^+$), Percentages of immune cell populations within $CD45^+$ cells are shown at the right panel (n = 6). (I) tSNE analysis by Flowjo for memory or exhaustion T cell subpopulation; T_{EM} ($CD8^+CD44^+CD69^-CD62L^-$), T_{CM} ($CD8^+CD44^+CD69^-CD62L^+$), T_{RM} ($CD8^+CD44^+CD69^+CD62L^-$), Tmem ($CD4^+CD44^{hi}CD62L^{hi}$), TeffTmem ($CD4^+\ CD44^{hi}CD62L^{lo}$), Tn ($CD4^+\ CD44^{lo}CD62L^{hi}$), TIM-$3^+$ T cells ($CD8^+TIM\text{-}3^+$), LAG-3^+ T cells ($CD8^+LAG3^+$), PD-1^+ T cells ($CD8^+PD\text{-}1^+$), CTLA-4^+ T cells ($CD8^+CTLA\text{-}4^+$), (J) Percentages of immune cell populations within $CD3^+$ cells are shown (n = 6). (K) Representative tumor images from the orthotopic HCC model treated using Clophosome or anti-CD8. (L) Tumor weight analysis from the orthotopic HCC model treated using Clophosome or anti-CD8 (n = 4 mice per group). (M) Survival curve of the mice from the orthotopic HCC model treated by Clophosome or anti-CD8 (n = 10 mice per group). Error bars represent the Mean ± SEM. Statistical analyses were performed using Student *t* test, one-way ANOVA, and two-way ANOVA with Tukey multiple comparisons test, and Log-rank test, $*p < 0.05$, $**p < 0.01$, $***p < 0.001$. Abbreviations: NCG, NOD/ShiLtJGpt-Prkdcem26Cd52Il2rgem26Cd22/Gpt; ND, normal diet; STS, short-term starvation; T_{CM}, central memory T cell; T_{EM}, effector memory T cells; T_{RM}, tissue-resident memory T cells.

conditions onto the left flank (immunization side) of C57BL/6J mice (immunocompetent) and NCG (NOD/ShiLtJGpt-Prkdcem26Cd52Il2rgem26Cd22/Gpt) mice (immunodeficient). After 1 week, all mice were inoculated with normally cultured HCC cells on the right flank (naive tumor side) (Figure 2A). Although low-nutrient conditions suppressed tumor cell migration and proliferation (Supplemental Figures S3A–L, http://links.lww.com/HEP/J715), we observed no differences in tumor growth. However, when the above mice were subjected to the STS regimen, tumor growth was inhibited in immunocompetent mice but not in immunodeficient mice regardless of the previous culture conditions (Figures 2B–E; Supplemental Figures S4A–H, http://links.lww.com/HEP/J715). This finding suggests that STS suppresses HCC regression by regulating the immune system.

To further determine how STS regulates the HCC immune microenvironment, we performed transcriptomic analysis by RNA-sequencing using the tumor mass from the orthotopic HCC model. The STS group had higher scores for macrophages and $CD8^+$ T cells (Figure 2F). STS altered TAM polarization from pTAMs to aTAMs, whereas no notable changes were observed in the ratio of other immune cells (Figure 2G). The ratio of $CD8^+IFN\gamma^+$ T cells and $CD8^+$Granzyme B^+ T cells ($GZMB^+$ T cells) was elevated in the STS group from the orthotopic and hydrodynamic HCC models (Figure 2H; Supplemental Figures S5A–E, http://links.lww.com/HEP/J715). Moreover, STS increased the frequency of effector memory T cells and decreased the expression of immune checkpoint molecules including T-cell immunoglobulin and mucin domain-3 (TIM-3) and lymphocyte activation gene-3 (LAG-3) (Figures 2I, J). Specific immune cell clearance experiments demonstrated that STS improved the immune microenvironment, dependent on macrophages and $CD8^+$ T cells (Figures 2K–M).

Next, we assessed changes in major myeloid and T cell populations in the blood and bone marrow (BM) of healthy and tumor-bearing mice (Supplemental Figure S6A, http://links.lww.com/HEP/J715). STS inhibited $CD8^+$ T cell and central memory T cell (T_{CM}) accumulation in the blood and increased the numbers of $CD4^+$ T cells, $CD8^+$ T cells, and T cell and central memory T cell in the BM (Supplemental Figures S6B–E, http://links.lww.com/HEP/J715). A decline in effector memory T cell was observed in the BM, but significant accumulation was observed in the blood (Supplemental Figure S6E, http://links.lww.com/HEP/J715). Moreover, we observed a significant enhancement in $CD45^+CD11b^{hi}Gr1^{hi}$ myeloid-derived suppressor cells (G-MDSCs) in tumor-bearing mice compared to that in healthy mice (Supplemental Figures S6F, G, http://links.lww.com/HEP/J715). Notably, STS decreased the number of G-MDSCs and $CD45^+CD11b^{hi}Gr1^{mid}$ myeloid-derived suppressor cells (M-MDSCs) in blood. In contrast to the other compartments examined, G-MDSCs and M-MDSCs increased in the BM during STS (Supplemental Figures S6F, G, http://links.lww.com/HEP/J715). The observed alterations in MDSC populations were consistent with previous evidence that monocytes can reenter the BM during fasting.[10] Moreover, elevated numbers of $CD11b^{hi}Gr1^{lo}$ macrophages were observed in both blood and BM (Supplemental Figure S6F, G, http://links.lww.com/HEP/J715).

Taken together, our findings suggest that STS can inhibit HCC tumor growth by stimulating the polarization of macrophages toward aTAMs and enhancing $CD8^+$ T cell function. Moreover, STS augmented the intratumoral

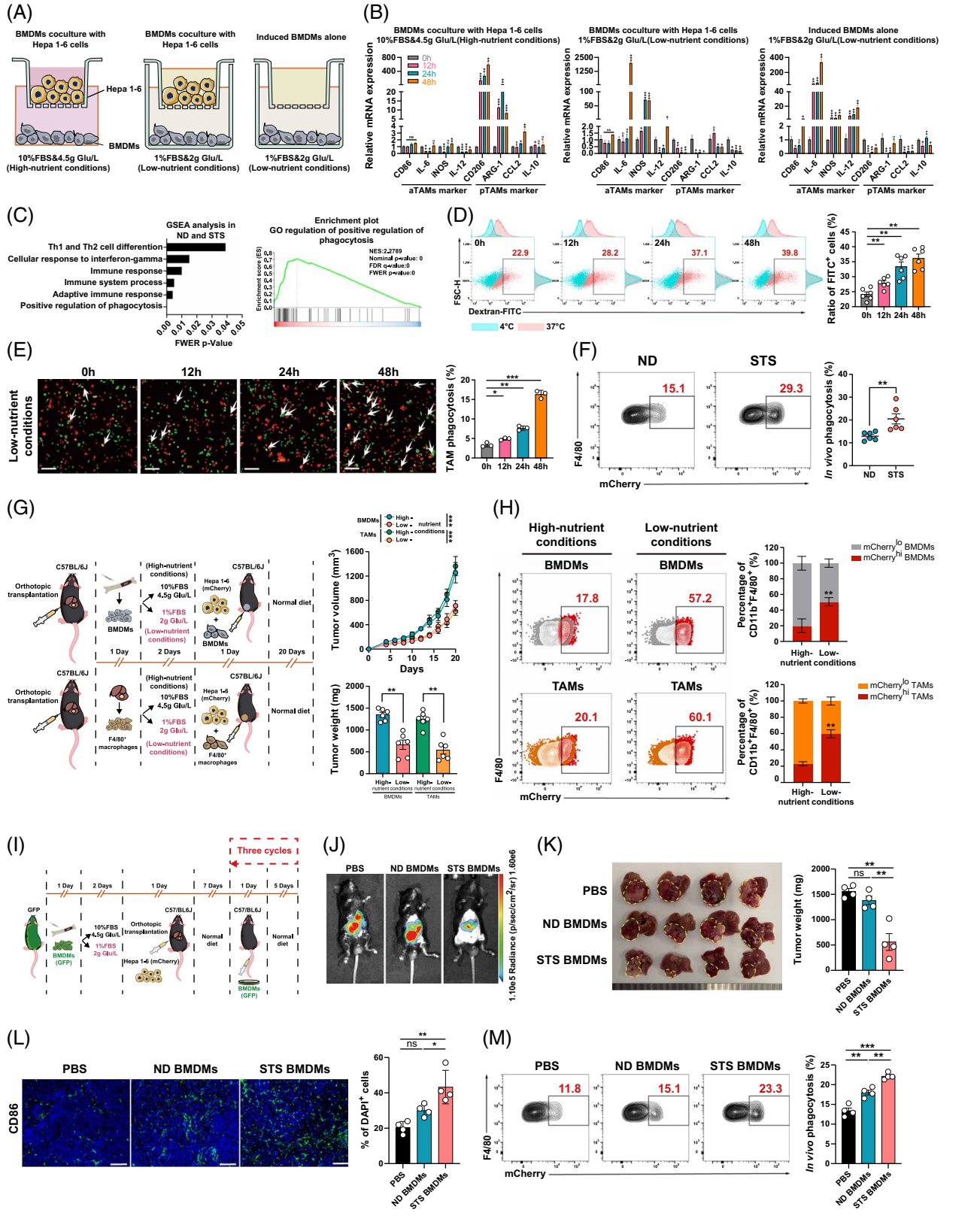

FIGURE 3 STS expedites macrophage polarization to aTAMs and enhances macrophage phagocytosis. (A) A co-culture system of murine macrophages BMDMs (bottom) and Hepa1-6 cells (top). Left: high-nutrient conditions (10% FBS and 4.5 g Glu/L); middle: low-nutrient conditions (1% FBS and 2 g Glu/L); right: culturing BMDMs alone under low-nutrient conditions. (B) Relative expression of the indicated genes using qPCR. (C) The top 6 immuno-related GSEA pathways from the transcriptome of the orthotopic HCC model and the positive regulation of phagocytosis, are presented for both the ND and STS groups. (D) BMDMs were incubated with 1 mg/mL dextran-FITC molecules for 60 minutes at 4°C or at 37°C, and the percentage of FITC$^+$ cells and MFI of FITC on F4/80$^+$ cells were measured using flow cytometry. Red: macrophage engulfing FITC

molecules. Blue: macrophage without FITC molecules. (E) A co-culture system of both CFSE-labeled BMDMs and PKH26-stained Hepa1-6 cells was subjected to starvation for 0, 12, 24, and 48 hours (n = 3). Debris and dead cells are washed by PBS. Representative images and the percentage of macrophages engulfing tumor cells in the visual field are shown. Green: BMDMs; Red, Hepa1-6 cells. White asterisks denote the macrophages engulfing tumor cells. Magnification×20, scale bar = 100 μm. (F) Statistic analysis and representative histograms showing intratumoral TAMs that phagocytic tumor cells from ND and STS groups. mCherry^{hi} TAMs were considered to be phagocytosing (n = 6). (G) Schematic diagram of the experimental approach and statistical analysis of tumor weight or size. BMDMs or F4/80$^+$ macrophages (TAMs) from tumor-bearing mice pretreated by high or low-nutrient conditions were mixed with Hepa 1-6-mCherry-luc$^+$ cells and inoculated in the left flank of C57BL/6J mice. (H) Statistical analysis and representative histograms show the phagocytosis of intratumoral macrophages, mCherry^{hi} TAM was considered to be phagocytosing (n = 4). (I) Schematic diagram of the experimental approach. BMDMs from GFP-positive mice pretreated by high or low-nutrient conditions were injected intravenously into C57BL/6J mice with tumors, 3 injections every 6 days. (J) In vivo bioluminescent imaging (BLI) of tumor growth in the orthotopic HCC model at the experimental endpoint. (K) Gross tumor images and weight statistics of mice undergoing macrophage adoptive therapy (n = 4 mice per group). (L) Representative immunofluorescence images and analysis of CD86 from the tumor (n = 4). (M) Statistical analysis and representative histograms show the phagocytosis of intratumoral macrophages (n = 4). Error bars represent the Mean ± SEM. Statistical analyses were performed using Student *t* test, one-way ANOVA, and 2-way ANOVA with Tukey multiple comparisons test. $^*p < 0.05$, $^{**}p < 0.01$, $^{***}p < 0.001$. Abbreviations: aTAMs, antitumoral TAMs; BMDMs, bone marrow-derived macrophages; GSEA, Gene set enrichment analysis; ND, normal diet; pTAMs, protumoral TAMs; STS, short-term starvation; TAMs, tumor-associated macrophages.

immune memory response and rearranged the systemic immune cell pool.

STS orchestrates TAM reprogramming and activates aTAMs to phagocytose tumor cells

To explore the direct effect of STS on TAMs, we analyzed the mRNA levels of bone marrow-derived macrophages (BMDMs) by co-culturing them with Hepa1-6 tumor cells under high or low-nutrient conditions (Figure 3A). Starvation-induced antitumor polarization under low-nutrient conditions (Figure 3B; Supplemental Figures S7A, B, http://links.lww.com/HEP/J715). Moreover, STS supported the progression to a STAT1-dependent antitumoral phenotype but inhibited STAT6-mediated protumoral phenotype activation (Supplemental Figure S7C, http://links.lww.com/HEP/J715). The observed stable morphology and greater tolerance indicated that macrophage function remained unaffected by starvation (Supplemental Figures S8A–F, http://links.lww.com/HEP/J715). Gene set enrichment analysis results, and phagocytosis assays suggested augmented phagocytic activity of macrophages in the STS group (Figures 3C–F).

To further explore whether STS enhances the tumoricidal capacity of TAMs in vivo, BMDMs extracted from BM and F4/80$^+$ TAMs from tumor tissues were cultured under high and low-nutrient conditions, respectively (Figure 3G). Tumor growth was slower, and tumor size was reduced in Hepa1-6 plus BMDMs or F4/80$^+$ TAMs precultured under low-nutrient conditions (Figure 3G, H; Supplemental Figures S9A–D, http://links.lww.com/HEP/J715). To verify whether macrophages undergoing STS intervention exhibited long-lasting antitumor effects in the TME, we conducted a pulse-chase experiment involving the adoptive transfer of GFP$^+$ BMDMs into mice bearing mCherry labeled tumor cells (Figure 3I; Supplemental Figure S9E, http://links.lww.com/HEP/J715). The infusion of BMDMs precultured under low-nutrient conditions suppressed HCC tumor growth compared to the other treatment groups (Figures 3J, K). Furthermore, an increased number of antitumoral macrophages were observed in the liver of mice that received adoptive macrophage transfer therapy (Figure 3L). Notably, the phagocytic ability of the STS-pretreated macrophages remained intact in vivo (Figure 3M). Rag2$^{-/-}$ mice displayed reduced tumor growth compared to those receiving BMDMs cultured under high-nutrient conditions (Supplemental Figures S10A–F, http://links.lww.com/HEP/J715). These findings imply that starvation expedites the transformation of pTAMs into aTAMs and enhances their ability to phagocytose tumor cells.

TAMs modulated by STS potentiate antitumor CD8$^+$ T cell responses

The direct effects of STS on CD8$^+$ T cells remain unclear. However, CD8+ T cells isolated from the spleen of OT-1 mice effectively secreted GZMB and IFNγ and killed Hepa1-6 cells, but these effects were inhibited under STS-like conditions. Notably, the antitumor activity was further enhanced by adding BMDMs to CD8$^+$ T cells cultured under low-nutrient conditions (Figures 4A–C). Furthermore, we used an ex vivo autologous cytotoxic system with CD8$^+$ T cells and F4/80$^+$ macrophages (TAMs) derived from Hepa1-6 hepatoma-bearing mice, following a previously described protocol (Supplemental Figures S11A, B, http://links.lww.com/HEP/J715).[23] Hepa1-6 cells co-cultured with CD8$^+$ T cells from STS mice were more apoptotic, suggesting that the STS regimen confers CD8$^+$ T cells in vivo with a more potent antitumor activity. The killing capacity of CD8$^+$ T cells purified from tumors treated with macrophage scavenger Clophosome was considerably attenuated. Consistently, co-culture assays performed with the addition of TAMs or BMDMs demonstrated an increase in the number of apoptotic tumor cells (Supplemental Figure S11C, D, http://links.lww.com/HEP/J715).

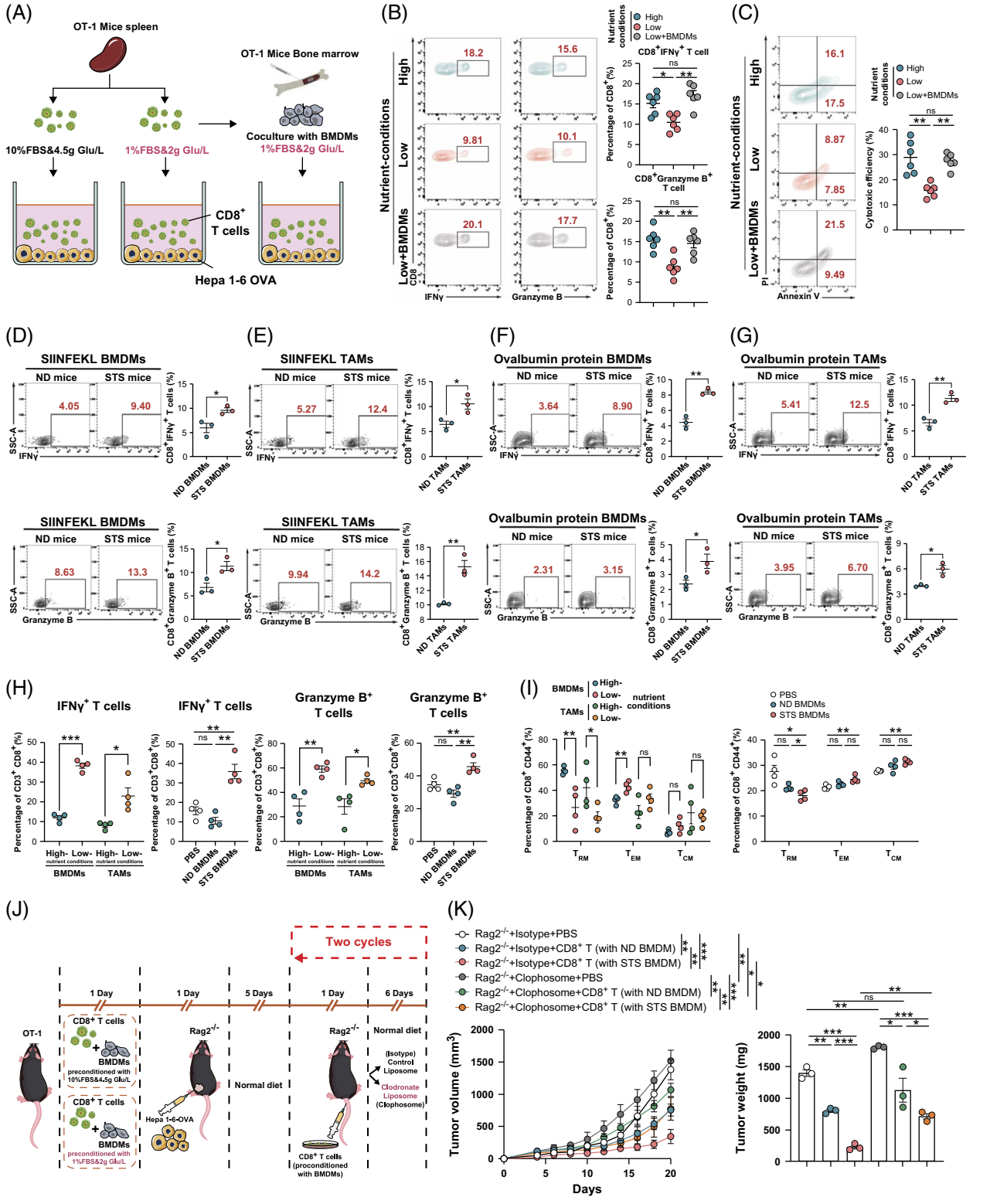

FIGURE 4 STS-mediated TAMs improve CD8$^+$ T cells-mediated cytotoxic and memory response. (A) A co-culture system of Hepa 1-6 cells and CD8$^+$ T cells or BMDMs from OT-1 mice. (B) The functional state of CD8$^+$ T cells was analyzed using flow cytometric quantification of GZMB$^+$ and IFNγ^+ cells (n = 6). (C) of Hepa1-6 cells caused by CD8$^+$ T cells was measured following Annexin V-PI staining (n = 6). (D–G) Representative plots and percentages of IFNγ or GZMB -producing OT-1 CD8$^+$ T cells co-cultured with the SIINFEKEL peptide or the OVA protein-loaded BMDMs or F4/80$^+$ TAMs isolated from tumor-bearing mice (n = 3). (H) The functional state of the T-cell subpopulation from tumor-bearing mice was analyzed by flow cytometric quantification. The sample includes tumor tissue from inoculation of BMDMs or F4/80$^+$ TAMs pretreated by high or low-nutrient conditions and Hepa 1–6 cells or tumor tissue treated by BMDMs adoptive therapy (n = 4). (I) Memory T cell subpopulation was analyzed by flow cytometric quantification (n = 4). (J) Schematic diagram of the experimental approach. Rag2$^{-/-}$ mice bearing Hepa1-6-OVA were

injected intravenously with $CD8^+$ T cells co-cultured with BMDMs pretreated with high-nutrient or low-nutrient conditions on days 6 and 13. These mice were treated with clodronate liposome or control liposome post-$CD8^+$ T cells adoptive therapy. (K) Tumor weight or size statistics of mice $Rag2^{-/-}$ mice bearing Hepa1-6-OVA treated by $CD8^+$ T cells or clodronate liposome (n = 3 mice per group). Error bars represent the mean ± SEM. Statistical analyses were performed using Student *t* test, one-way ANOVA with Tukey multiple comparisons test, and two-way ANOVA, $^*p < 0.05$, $^{**}p < 0.01$, $^{***}p < 0.001$. Abbreviations: BMDMs, bone marrow-derived macrophages; ND, normal diet; STS, short-term starvation; TAMs, tumor-associated macrophages.

Macrophages can favor T-cell–mediated antitumor responses by secreting cytokines or presenting tumor antigens on major histocompatibility complex class I/II.[33] $CD8^+$ T cells co-cultured with the supernatant from STS-conditioned BMDMs secreted more GZMB and IFNγ (Supplemental Figures S12A, B, http://links.lww.com/HEP/J715). Moreover, an antigen presentation assay demonstrated that BMDMs or TAMs treated with STS-like conditions cross-primed $CD8^+$ T cells for both the SIINFEKL peptide and the OVA protein better than their high-nutrient conditioned counterparts, as evident by their increased production of GZMB and IFNγ (Figures 4D–G). However, fasting did not affect the inhibitory activity of MDSCs or the cross-priming capacity of DCs (Supplemental Figures S12C–F, http://links.lww.com/HEP/J715). Moreover, $CD8^+$ T cells exhibited enhanced cytokine secretion and an immune memory phenotype in STS-preconditioned macrophages (Figures 4H, I).

To further verify that fasting-modified macrophages are sufficient to regulate the antitumor response of $CD8^+$ T cells in vivo, Hepa1-6-OVA cells inoculated into $Rag2^{-/-}$ mice and treated with $CD8^+$ T cells from OT-1 mice cultured with STS BMDMs showed reduced tumor growth compared to those injected with $CD8^+$ T cells cultured with ND BMDMs or PBS. Nevertheless, the tumors of $Rag2^{-/-}$ mice that received macrophage scavengers grew more rapidly (Figures 4J, K; Supplemental Figure S13, http://links.lww.com/HEP/J715). Thus, TAMs reprogrammed with STS can enhance the antitumor capacity of $CD8^+$ T cells.

Combination treatment of STS with anti-PD-L1 shows superior effects compared to combinatorial treatment with anti-PD-1

The combined efficacy of dietary therapy and immunotherapy in HCC remains unknown. To study this, we divided the mice into 6 groups and administered ND, STS, anti-PD-1, anti-PD-L1, STS+anti-PD-1, or STS +anti-PD-L1 in both subcutaneous and orthotopic HCC models (Figures 5A, B; Supplemental Figure S14A, http://links.lww.com/HEP/J715). Tumor growth and body weight were monitored (Supplemental Figures S14A–E, http://links.lww.com/HEP/J715). The combination of STS with anti-PD-L1 reduced the tumor burden more than the combination of anti-PD-1 or other therapies alone (Figure 5B; Supplemental Figures S14A, D, http://links.lww.com/HEP/J715). The survival analysis revealed that STS combined with anti-PD-L1 therapy had the highest efficacy (Figure 5B; Supplemental Figures S14B, E, http://links.lww.com/HEP/J715). These findings prompted us to explore the effectiveness of STS combined with ICIs and its correlation with the therapy cycle length. Therefore, based on the initial 3 cycles, we expanded the treatment to include one additional cycle of STS and anti-PD-1/L1 cycle. The results demonstrated that this combined regimen effectively sensitized the tumor to anti-PD-1 during the 4 cycles. The combination of STS with anti-PD-L1 still exhibited superior effects (Supplemental Figure S14F, http://links.lww.com/HEP/J715).

To evaluate the effects of individual or combined treatments on the HCC immune microenvironment, we examined the immunophenotypes of tumor-infiltrating immune cells. Starvation alone caused the upregulation of aTAMs infiltration and a decrease in pTAMs (Figure 5C; Supplemental Figure S15A, http://links.lww.com/HEP/J715). No significant differences were detected in the percentages of other immune cell populations, such as MDSCs, regulatory T cells, total $CD4^+$ T cells, total $CD8^+$ T cells, or dendritic cells (Supplemental Figure S15B, http://links.lww.com/HEP/J715). The strongest capacity to produce effector cytokines such as IFNγ or GZMB was observed in the STS combined with the anti-PD-L1 group compared with other groups (Figure 5D; Supplemental Figures S15B, C, http://links.lww.com/HEP/J715). In addition, STS combined with PD-L1 caused a significant decrease in the frequency of (tissue-resident memory) T_{RM} and an increase in effector memory T cells (Figure 5E). Consistently, the tumor size treated with combined depletion of $CD8^+$ T cells and TAMs closely resembled the initial tumor size of the ND group (Figures 5F, G; Supplemental Figure S16, http://links.lww.com/HEP/J715).

Taken together, the combination of STS and ICIs has an optimal effect on reducing tumor growth and increasing HCC tumor survival. Combinatorial therapy, similar to starvation therapy alone, activates aTAMs and $CD8^+$ T cell killing function and provides long-lasting immune memory responses.

ExoPD-L1 from TAMs impairs the efficacy of anti-PD-1/L1

Our results demonstrated that STS enhances the efficacy of anti-PD-1/PD-L1 therapy. These findings

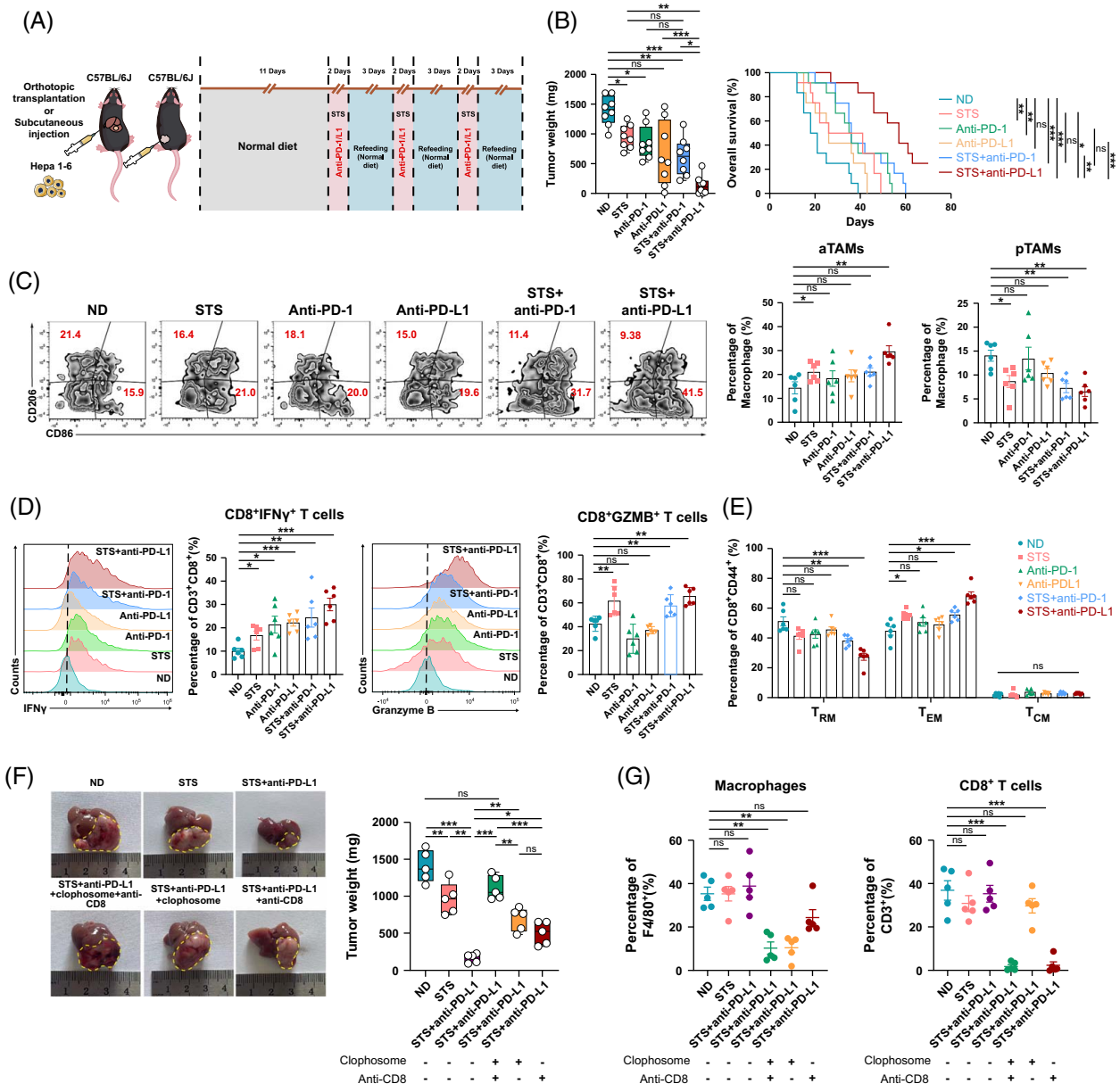

FIGURE 5 Effect of STS combined with anti-PD-L1 is superior to anti-PD-1. (A) Schematic diagram of the experimental approach. (B) Tumor weight statistics and survival curve of the orthotopic HCC model mice undergoing single regimen or combined therapy (n = 8–10 mice per group). (C) Representative plots and percentages of TAMs in the orthotopic HCC model from the ND, STS, anti-PD-1, anti-PD-L1, STS combined with anti-PD-1, and STS combined with anti-PD-L1 groups (n = 6). (D) Statistical analysis and representative histograms show the functional state of $CD8^+$ T cells in 6 groups (n = 6). (E) Statistical analysis of memory $CD8^+$ T-cell subpopulations in 6 groups (n = 6). (F) Gross tumor images and tumor weight analysis from the orthotopic HCC model from the ND group, STS group, and STS combined with anti-PD-L1 group treated by Clophosome or anti-CD8 (n = 5 mice per group). (G) Statistical analysis of $CD8^+$ T cell and $F4/80^+$ macrophage clearance from mice treated with STS or STS combined with anti-PD-L1. Error bars represent the mean ± SEM. Statistical analyses were performed using one-way ANOVA with Tukey multiple comparisons test and Log-rank test, $^*p < 0.05$, $^{**}p < 0.01$, $^{***}p < 0.001$. Abbreviations: aTAMs, antitumoral TAMs; ND, normal diet; PD-L1, programmed cell death ligand 1; pTAMs, protumoral TAMs; STS, short-term starvation; TAMs, tumor-associated macrophages.

prompted us to explore the mechanisms by which STS sensitizes tumors to ICIs. Consequently, we investigated the distributions of PD-1 and PD-L1 expression in the orthotopic HCC model. Compared to the blood and spleen, PD-1 and PD-L1 were mainly expressed in the tumor tissue by lymphocytes and myeloid cells (Figures 6A, B). In addition, PD-1/PD-L1 expression was mainly enriched in TAMs compared with other myeloid cells (Figures 6C, D). Western blotting studies demonstrated that STS downregulated PD-L1 expression, but not PD-1, in tumor tissues (Supplemental Figure S17A, http://links.lww.com/HEP/J715). Therefore, PD-L1 expression, specifically in TAMs, may influence the efficacy of ICI therapies.

Macrophage-derived exosomes contain abundant exoPD-L1 levels.[34] Moreover, tumor cell-derived

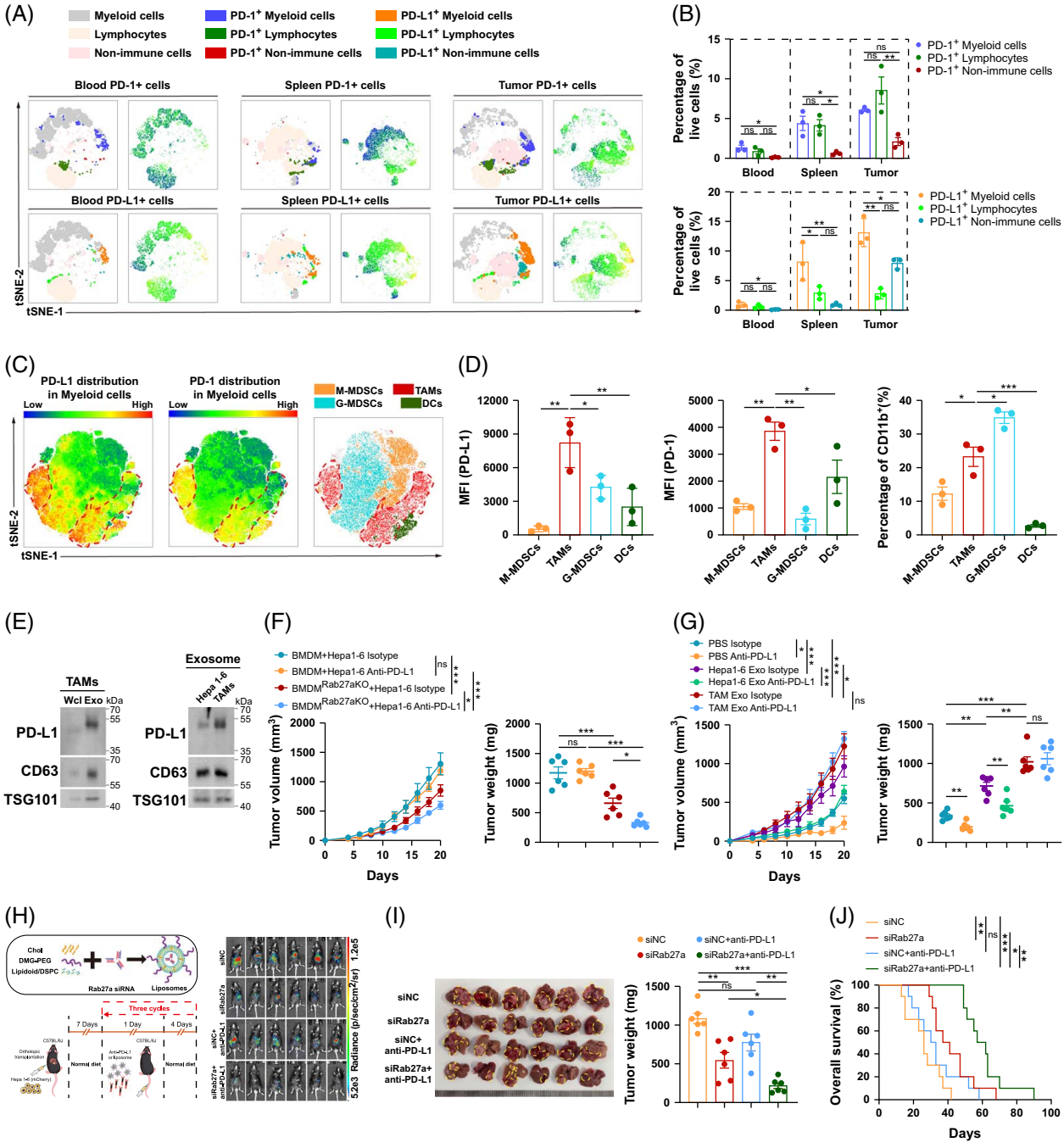

FIGURE 6 exoPD-L1 is enriched in TAMs and participates in anti-PD-1/L1 resistance. (A) tSNE map derived from flow cytometric analysis indicating the populations of the infiltrating PD-1$^+$ or PD-L1$^+$cells in blood, spleen, and tumor tissue. (B) Statistical analyses of PD-1$^+$ or PD-L1$^+$ myeloid cells (CD45$^+$CD11b$^+$), lymphocytes (CD45$^+$CD11b$^-$), and nonimmune cells (CD45$^-$) in blood, spleen, and tumor tissue (n = 3). (C) tSNE analysis by Flowjo for the expression of PD-1$^+$ or PD-L1$^+$ in myeloid cells including G-MDSC (CD11b^{hi}Gr1^{hi}F4/80$^-$), TAMs (CD11b^{hi}Gr1^{hi}F4/80$^+$), M-MDSC (CD11b^{hi}Gr1^{mid}F4/80$^-$), and DCs (CD11b^{hi}Gr1^{lo}F4/80$^-$CD11c$^+$IA/IE$^+$). The red areas represent TAMs. (D) Statistical analyses and percentage of PD-1$^+$ or PD-L1$^+$ myeloid cell and percentage of myeloid cell populations within CD11b$^+$ cells (n = 3). (E) Left: the protein levels of PD-L1, CD63, and TSG101 in whole-cell lysate (Wcl) and exosomes (Exo) from TAMs. Right: the exosome protein levels of PD-L1, CD63, and TSG101 in Hepa1-6 and TAMs. (F) Tumor weight or size statistics from mice inoculated with Hepa1-6 mixed with BMDMs (Rab27a KO or WT) (n = 6 mice per group). All mice were treated with anti-PD-L1 or isotype. (G) Tumor weight or size statistics from mice inoculated with Hepa1-6 (Rab27a KO) mixed with BMDMs (Rab27a KO) All mice were treated with anti-PD-L1 or isotype. Some mice were injected intravenously with Hepa1-6 exosome (Hepa1-6 Exo) or TAM exosome (TAM Exo) (n = 6 mice per group). (H) Schematic diagram showing the preparation of Rab27a siRNA-loaded liposomes and experimental approach and BLI of tumor growth. (I) Gross tumor images and tumor weight analysis of mice received liposome or anti-PD-L1 (n = 6 mice per group). (J) Survival curve of siNC group, siRab27a group, siNC+anti-PD-L1 group, and siRab27a+anti-PD-L1 group (n = 6 mice per group). Error bars represent the Mean ± SEM. Statistical analyses were performed using one-way ANOVA and two-way ANOVA with Tukey multiple comparisons test, and Log-rank test, *$p < 0.05$, **$p < 0.01$, ***$p < 0.001$. Abbreviations: DC, dendritic cell; DMG-PEG, dimyristoyl glycerol-polyethylene glycol; MDSCs, myeloid-derived suppressor cells; PD-L1, programmed cell death ligand 1; TAMs, tumor-associated macrophages.

exoPD-L1 attenuates the efficacy of PD-L1 antibodies.[30] We hypothesized that macrophage-derived exoPD-L1 impairs ICI efficacy. We found that PD-L1 was mainly expressed in TAM exosomes. Furthermore, TAM exosomes expressed more PD-L1 than tumor cells (Figure 6E). Using genetic knockouts of Rab27a in TAMs, we found that exosomal PD-L1 expression decreased significantly (Supplemental Figure S17B, http://links.lww.com/HEP/J715). TAMs Rab27a-KO not only suppressed tumor growth but also enhanced the efficacy of anti-PD-L1 in the tumor (injection of TAMs Rab27aKO combined with Hepa 1–6 cells) (Figure 6F; Supplemental Figure S17C, http://links.lww.com/HEP/J715). Nevertheless, Rab27a-KO tumor cells did not affect the anti-PD-L1 in tumor efficacy (injection of TAMs combined with Hepa 1–6 cells Rab27aKO) (Supplemental Figure S17E, http://links.lww.com/HEP/J715). Next, we injected exosomes from tumor cells and TAMs into mice bearing tumor, including Rab27a-KO tumor cells and BMDMs. The injection of TAM-derived exosomes promoted tumor growth more than tumor cells and contributed to PD-L1 antibody resistance (Figure 6G; Supplemental Figure S17D, http://links.lww.com/HEP/J715). Moreover, TAMs Rab27a-KO enhanced the anti-PD-1 efficiency (Supplemental Figure S17F, http://links.lww.com/HEP/J715). Although exosomes derived from TAMs promoted tumor growth and ICI resistance, supplementation with TAMs-PD-L1 KO exosomes did not resist the effect of anti-PD-1/L1 treatment (Supplemental Figure S17G, H, http://links.lww.com/HEP/J715).

Liposomes are known to target macrophages and act as synergistic therapies in combination with ICIs.[35] Interestingly, targeting siRab27a directly inhibited tumor growth. Furthermore, siRab27a liposomes combined with PD-L1 antibodies demonstrated better efficacy and increased survival (Figures 6H–J). The above results showed that PD-L1 was mainly enriched in TAMs and that TAMs were the main source of exoPD-L1 and caused ICI resistance. Suppression of exosomal secretion from TAMs can enhance the efficacy of the PD-1/L1 antibody.

Starvation attenuates exoPD-L1 secretion in TAMs through the FBP1/Akt/mTOR/Rab27a axis

We evaluated the Rab27a and exoPD-L1 expression in TAMs under different nutritional conditions. STS suppressed Rab27a and inhibited exoPD-L1 secretion (Figures 7A, B; Supplemental Figure S18A, http://links.lww.com/HEP/J715). Rab27a is a key factor regulating exosome secretion by macrophages (Supplemental Figure S18B, http://links.lww.com/HEP/J715). Until recently, the relationship between metabolic changes and the regulation of exosome secretion and immune checkpoint levels remained poorly understood. Therefore, we analyzed changes in several metabolic pathways via transcriptomics and found a significant upregulation of the key gluconeogenic enzyme fructose diphosphatase 1 (FBP1) in carbon metabolism (Figure 7C). FBP1 is mainly enriched in macrophages and tumor cells. The proportion of aTAMs increased in patients with high FBP1 expression (Figure 7D). We hypothesized that high FBP1 expression induced by STS causes Rab27a and exoPD-L1 downregulation. Tumor cells and macrophages were co-cultured under high-nutrient or low-nutrient conditions, and western blot analysis was performed (Figure 7E; Supplemental Figure S18C, http://links.lww.com/HEP/J715). A reduced expression of the key glycolytic enzymes hexokinase 2 and lactate dehydrogenase A under starvation conditions was noted. Moreover, glucose-6-phosphatase catalytic subunit 3 and FBP1 were upregulated in macrophages; however, no significant FBP1 upregulation was observed in tumor cells (Supplemental Figure S18C, http://links.lww.com/HEP/J715). Consistent with previous studies, starvation downregulated glycolysis and upregulated gluconeogenesis in tumor tissues (Supplemental Figure S18D, http://links.lww.com/HEP/J715).[6] To identify the altered metabolic enzymes responsible for the downregulation of Rab27a and exoPD-L1, we silenced and overexpressed the altered metabolic enzymes in TAMs subjected to STS. A significant Rab27a and exoPD-L1 downregulation was observed when FBP1 was overexpressed in TAMs (Figure 7E).

A negative correlation between FBP1 levels and Rab27a and exoPD-L1 expression in TAMs under different nutrient conditions was observed (Figure 7F). TAMs Rab27a-KO eliminate the effects of STS and FBP1 on exosome secretion (Supplemental Figure S18E, http://links.lww.com/HEP/J715). Previous research has shown that Akt is known to be involved in Rab27a-mediated TAM exosomal secretion.[34] Both published data and our results suggest a significant negative correlation between FBP1 and AKT downstream RICTOR expression and a positive correlation between mTOR and Rab27a (Supplemental Figure S18F, http://links.lww.com/HEP/J715). FBP1 can act as a dephosphorylase to perform nonmetabolic enzyme functions.[36] Our results suggested that FBP1 regulates Rab27a and exoPD-L1 expression by binding to Akt to suppress Akt/mTOR phosphorylation during ER (Figure 7G–I; Supplemental Figure S18G, http://links.lww.com/HEP/J715). Macrophages with high FBP1 levels exhibited a stronger tumor-inhibitory capacity (Supplemental Figure S19A–E, http://links.lww.com/HEP/J715). Inhibiting or activating AKT/mTOR activity by targeting FBP1-affected exoPD-L1 secretion via MK2206/Rapamycin or rIGF-1 (recombinant IGF receptor-1), respectively (Figure 7J). This process was mediated by Rab27a (Supplemental Figure S18H,

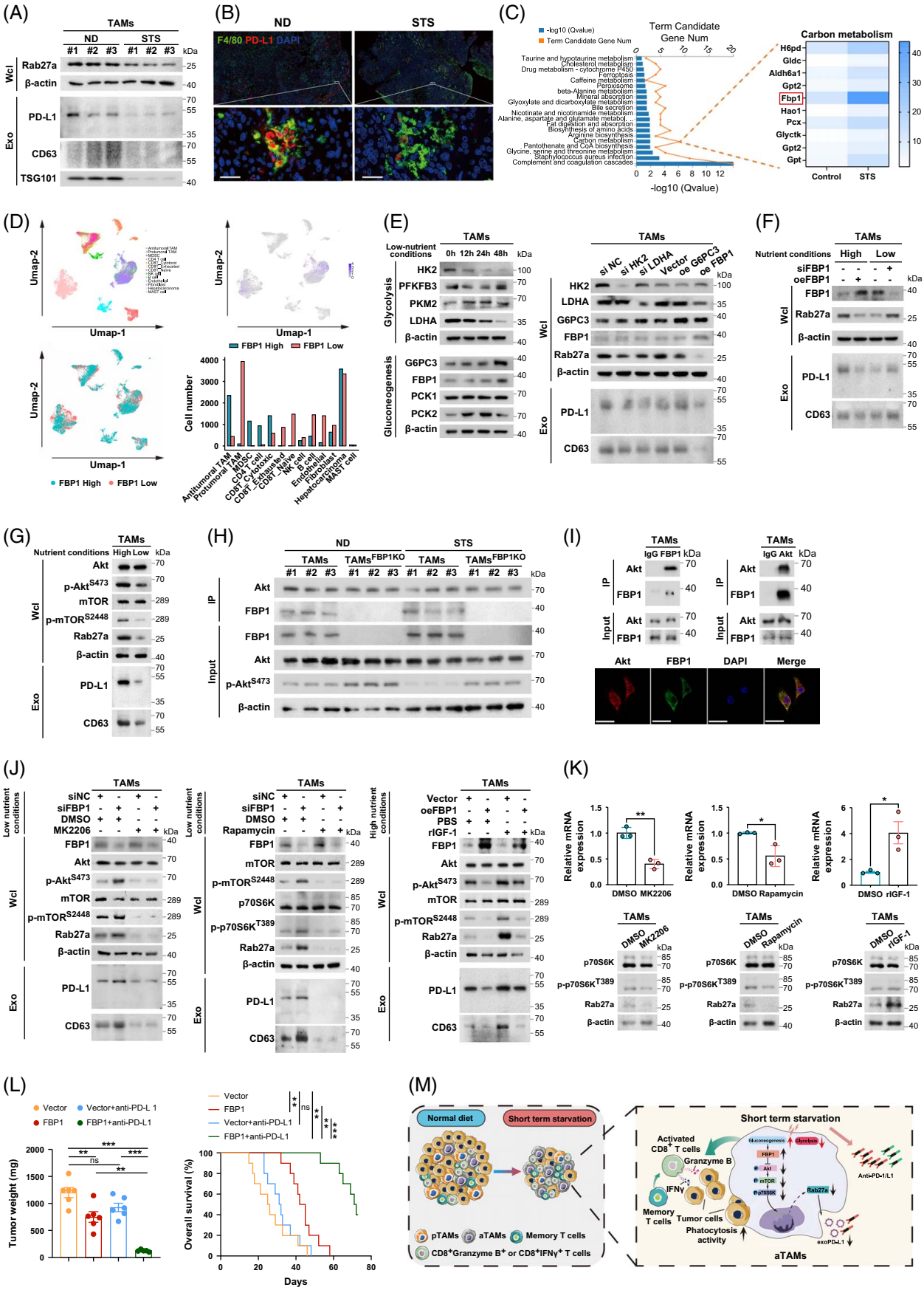
(A)
TAMs
ND
STS
#1 #2 #3 #1 #2 #3
kDa
Wcl
Rab27a
β-actin
Exo
PD-L1
CD63
TSG101
(B)
ND
STS
F4/80 PD-L1 DAPI
(C)
-log10 (Qvalue)
Term Candidate Gene Num
Term Candidate Gene Num
Taurine and hypotaurine metabolism
Cholesterol metabolism
Drug metabolism - cytochrome P450
Ferroptosis
Caffeine metabolism
Peroxisome
beta-Alanine metabolism
Mineral absorption
Glyoxylate and dicarboxylate metabolism
Bile secretion
Nicotinate and nicotinamide metabolism
Alanine, aspartate and glutamate metabol...
Fat digestion and absorption
Biosynthesis of amino acids
Arginine biosynthesis
Carbon metabolism
Pantothenate and CoA biosynthesis
Glycine, serine and threonine metabolism
Staphylococcus aureus infection
Complement and coagulation cascades
-log10 (Qvalue)
Carbon metabolism
H6pd
Gldc
Aldh6a1
Gpt2
Fbp1
Hao1
Pcx
Glyctk
Gpt2
Gpt
Control
STS
(D)
Umap-1
Umap-2
FBP1 High
FBP1 Low
Cell number
Antitumoral TAM
Protumoral TAM
MDSC
CD4_Cytotoxic
CD8T_Exhausted
CD8T_Naive
NK cell
B cell
Endothelial
Fibroblast
Hepatocarcinoma
MAST cell
(E)
TAMs
Low-nutrient conditions
0h 12h 24h 48h
kDa
Glycolysis
HK2
PFKFB3
PKM2
LDHA
β-actin
Gluconeogenesis
G6PC3
FBP1
PCK1
PCK2
β-actin
si NC
si HK2
si LDHA
Vector
oe G6PC3
oe FBP1
Wcl
Exo
(F)
TAMs
Nutrient conditions
High
Low
siFBP1
oeFBP1
(G)
TAMs
Nutrient conditions
High Low
Akt
p-Akt S473
mTOR
p-mTOR S2448
(H)
ND
STS
TAMs
TAMs FBP1KO
IP
Input
(I)
TAMs
IgG FBP1
IgG Akt
Akt
FBP1
DAPI
Merge
(J)
TAMs
Low nutrient conditions
High nutrient conditions
siNC
siFBP1
DMSO
MK2206
Rapamycin
Vector
oeFBP1
PBS
rIGF-1
p-p70S6K T389
p70S6K
Rab27a
(K)
Relative mRNA expression
DMSO MK2206
DMSO Rapamycin
DMSO rIGF-1
(L)
Vector
Vector+anti-PD-L 1
FBP1
FBP1+anti-PD-L1
Tumor weight (mg)
Overall survival (%)
Days
(M)
Normal diet
Short term starvation
pTAMs
aTAMs
Memory T cells
CD8+Granzyme B+ or CD8+IFNγ+ T cells
Activated CD8+ T cells
Granzyme B
IFNγ
Memory T cells
Tumor cells
Phatocytosis activity
Anti-PD-1/L1
exoPD-L1
aTAMs

FIGURE 7 STS inhibits Rab27a and exoPD-L1 of TAMs through activating FBP1 (A) TAMs were isolated from mice subjected to ND or STS diet. The protein levels show Rab27a in Wcl and PD-L1, CD63, and TSG101 in exosomes (Exo). (n = 3 mice per group) (B) Representative immunofluorescent staining for F4/80$^+$ or PD-L1$^+$ cells from mice undergoing ND or STS regimen. F4/80 (green), PD-L1 (red), and DAPI (blue), Magnification ×80, scale bar = 25 μm. (C) KEGG pathway analysis and term candidate gene number from the orthotopic HCC model with ND or STS assessed by RNA-seq (n = 3). The differences in FPKM values in carbon metabolism genes are shown in the right panel. (D) ScRNA-seq data (GSE149614) were analyzed. UMAP plots showing multiple cell clusters including antitumoral TAM, protumoral TAM, MDSC, CD4 T cell, CD8 T cytotoxic cell, CD8 T exhausted cell, CD8 T Naive cell, NK cell, B cell, Endothelial, Fibroblast, Hepatocarcinoma cell, MAST cell (left upper), the expression of FBP1 (right upper), FBP1 high and low origins (left lower) and cell proportion statistics (Right lower panel). (E) Protein levels of the key enzymes in glycolysis (HK2, PFKFB3, PKM2, LDHA) and the key enzymes in gluconeogenesis (G6PC3, FBP1, PCK1, PCK2) were assessed by western blot in TAMs collected by the Hepa1-6 cells and BMDMs co-culture system (left). Protein levels of the indicated enzymes or exosomes following silencing HK2 and LDHA or overexpressing G6PC3 and FBP1 in TAMs (right). (F) The Rab27a and exoPD-L1 protein levels after silencing or overexpressing FBP1 in TAMs subjected to ND or STS-like conditions. (G) Protein levels of the Akt/mTOR pathway in TAMs subjected to ND or STS-like conditions. (H) Co-immunoprecipitation of FBP1 and Akt in TAMs or TAMs FBP1-KO isolated from mice subjected to ND or STS diet (n = 3). (I) Co-immunoprecipitation of FBP1 and Akt from BMDMs co-cultured with Hepa 1-6 cells (upper). Immunofluorescence assays for FBP1 (green) with Akt (red) in TAMs (below). Magnification ×80, scale bar = 25 μm. (J) Protein levels of the Akt/mTOR/Rab27a axis following silencing or overexpressing of FBP1 in TAMs added with MK2206, Rapamycin, and rIGF-1. (K) The mRNA expression of Rab27a and indicated protein levels in TAMs treated by MK2206, Rapamycin, and rIGF-1. (L) Tumor weight analysis and survival curve of four group mice (n = 6 mice per group). (M) Schematic diagram showing STS reshapes the TME by triggering a series of antitumor immune responses. Error bars represent the mean ± SEM. Statistical analyses were performed using Student *t* test, one-way ANOVA with Tukey multiple comparisons test, and Log-rank test, $^*p < 0.05$, $^{**}p < 0.01$, $^{***}p < 0.001$. Abbreviations: BMDMs, bone marrow-derived macrophages; ND, normal diet; STS, short-term starvation; TAMs, tumor-associated macrophages; Wcl, whole-cell lysate.

http://links.lww.com/HEP/J715). Blocking the AKT/mTOR pathway in TAMs impaired tumor progression, enhanced phagocytic potency, and activated CD8$^+$T cells (Supplemental Figures S20A–F, http://links.lww.com/HEP/J715). The downstream effector of mTORC1, P70S6 Kinase (P70S6K), correlated with Rab27a expression level (Figure 7K).

Furthermore, we synthesized a liposomal system capable of delivering the FBP1 overexpression plasmid to macrophages in vivo, as described.[37] FBP1 overexpression in macrophages combined with anti-PD-L1 treatment inhibited tumor growth and prolonged survival (Figure 7L; Supplemental Figures S21 A and B, http://links.lww.com/HEP/J715). In conclusion, STS suppresses Rab27a and exoPD-L1 levels by regulating the FBP1-mediated Akt/mTOR pathway, which enhances macrophage phagocytic potency and the subsequent antitumor effects of CD8$^+$ T cells. Enhancing FBP1 expression in TAMs can synergize the efficacy of anti-PD-L1.

DISCUSSION

This study provides new insights into the mechanism by which STS combined with ICIs causes HCC regression by regulating macrophage polarization toward antitumor phenotypes and augmenting CD8$^+$ T cell cytotoxicity. Moreover, STS enhanced the efficacy of PD-1/L1 antibodies by reducing the secretion of exoPD-L1 in macrophages. We further demonstrated that STS combined with anti-PD-L1 therapy had superior efficacy and improved survival compared with anti-PD-1 therapies. Macrophage metabolic reprogramming caused an FBP1-mediated reduction in Rab27a and exoPD-L1 expression via the Akt/mTOR axis, which enhanced phagocytosis and macrophage-dependent CD8$^+$ T cell function during STS (Figure 7M). Targeting Rab27a or overexpressing FBP1 could synergize with anti-PD-L1 treatment to reduce tumor burden. Our study provides robust preclinical evidence for the efficacy of the combination of nutritional therapy and immunotherapy in patients with HCC.

Evidence strongly suggests that ER modulates cancer immunosurveillance.[11,38,39] Several clinical trials have confirmed that fasting can reshape antitumor immunity.[8,40] This study demonstrated that STS induced tumor regression in multiple HCC models, suggesting that STS alone could suppress tumor growth. However, these findings were incongruent with previous studies.[2] Gastrointestinal cancers may respond differently to fasting compared to other cancers. The STS strategy used in our study appears to confer superior tumor regression effects compared to SCR in short-term regimens. Moreover, the improved survival of mice indicated that fasting could trigger effective and durable antitumor responses.

Memory T cells and monocytes re-enter the BM and alter the host response to antigen stimulation during transient external stressors.[10,41] These studies provided evidence that in a healthy body, immune cells tend to seek a “haven” in response to nutritional challenges. However, the mechanism by which STS modulates immune cell pools has been poorly investigated in patients with cancer or tumor-bearing mice. STS inhibited the levels of CD8$^+$ T cells, T cells, central memory T cells, G-MDSCs, and M-MDSCs in the blood and improved these levels in the BM. Moreover, CD11b^{hi}Gr1^{lo} macrophage accumulation was observed in both blood and BM. We further complemented and extended the conclusion that fasting induces tumor regression.

Although fasting-like conditions have been demonstrated to boost the proportion of cytotoxic CD8$^+$ T cells and NK cells and reduce Treg levels, starvation-

mediated antitumor immunity of macrophages is still poorly understood.[2,7,9,13,38] We provide sufficient evidence that STS enhanced the phagocytic potency of macrophages against tumor cells and promotes a switch in $CD8^+$ T cells toward an activated/memory phenotype.

Given that exoPD-L1 plays a significant role in ICI resistance, we confirmed that TAMs are the main source of exoPD-L1 and that they are involved in PD-1/L1 antibody tolerance. Inhibition of Rab27a alleviated the hijacking of PD-L1 antibodies by exoPD-L1 and increased its efficacy. Furthermore, combination treatment with STS and anti-PD-L1 showed superior effects when combined with anti-PD-1 in vivo. However, the combination efficiency of anti-PD-1 was not evident during the 3 fasting cycles. We speculate that this may be related to the treatment cycle, an additional mechanism of action of PD-L1 as a ligand, and changes in exosome levels during ICI therapy.[42] Therefore, we concluded that increased STS and anti-PD-1 cycles enhanced the efficacy of the combined regimen.

Fasting/FMD cycles can reshape cellular metabolism in TME.[12,43] Our results support the hypothesis that TAMs undergo metabolic reprogramming from glycolysis to gluconeogenesis with a concomitant decrease in exosomal secretion during nutrient restriction. FBP1 upregulation during carbon metabolism has also been observed. FBP1 expression consistently showed an inverse relationship with Rab27a and exoPD-L1 in macrophages and was correlated with their antitumor capacity. We noted that FBP1 induced dephosphorylation of Akt and its downstream effector molecules by binding to Akt. Moreover, Akt/mTOR activity suppression attenuated exoPD-L1 secretion and enhanced the antitumoral potency of macrophages. These results provide complementary evidence that enhancing FBP1 expression in macrophages is a potential therapeutic option. Our study had some limitations. For example, starvation conditions in vitro cannot fully simulate the microenvironment under STS conditions in vivo. The metabolites and intestinal flora are still unexplored during STS. Optimizing the simulated STS conditions in vitro and exploring the altered spectrum of metabolites and flora will be promising directions.

Our study provides important insights by demonstrating that STS suppresses the growth of multiple HCC types and reshapes the TME by triggering a series of antitumor immune responses centered on enhanced antitumoral potency and reduced exoPD-L1 secretion in TAMs. STS combined with ICIs induces optimal tumor regression and durable immunological memory responses, representing it as a promising adjuvant strategy for immunotherapy. Further testing and optimization should be continued to improve its compatibility for clinical development and usage.

DATA AVAILABILITY STATEMENT

The processed gene expression data of RNA-seq of HCC tumors during normal diet and short-term starvation are available at the GEO database under the accession code GSE291357.

AUTHOR CONTRIBUTIONS

Kun Cheng designed the study and contributed to the manuscript's writing. Kun Cheng and Ning Cai interpreted and analyzed the data. Kun Cheng, Ning Cai, and Xing Yang performed the experiments. Danfeng Li, Jinghan Zhu, Hui Yuan Yang, Sha Liu, and Deng Ning prepared figures and tables. Huifang Liang, Jianping Zhao, Zhanguo Zhang, and Wanguang Zhang initiated the study and revised the manuscript. Huifang Liang, Jianping Zhao, Zhanguo Zhang, and Wanguang Zhang accepted full responsibility for the study's work and/or conduct, had access to the data, and controlled the decision to publish. All the authors have read and approved the final manuscript.

ACKNOWLEDGMENTS

The authors thank several professional English editors (American and Chinese Journal Experts) for assistance in improving the quality of the language. The authors thank the scientific instruments and laboratory supplies from the Experimental Medicine Center, Tongji Hospital, Tongji Medical College, Huazhong University of Science and Technology, Wuhan 430030, People's Republic of China. The authors thank LetPub (http://www.letpub.com) and Editage (http://www.editage.com) for linguistic assistance and scientific consultation during the preparation of this manuscript.

FUNDING INFORMATION

This work was supported by The National Natural Science Foundation of China (No. 82373054 and 82173319 to Wanguang Zhang).

CONFLICTS OF INTEREST

The authors declare that they have no competing interests.

ORCID

Kun Cheng https://orcid.org/0000–0003–0742–1978
Wanguang Zhang https://orcid.org/0000–0003–3184–9907

REFERENCES

1. Taylor SR, Falcone JN, Cantley LC, Goncalves MD. Developing dietary interventions as therapy for cancer. Nat Rev Cancer. 2022;22:452–66.
2. Ajona D, Ortiz-Espinosa S, Lozano T, Exposito F, Calvo A, Valencia K, et al. Short-term starvation reduces IGF-1 levels to sensitize lung tumors to PD-1 immune checkpoint blockade. Nat Cancer. 2020;1:75–85.
3. Caffa I, Spagnolo V, Vernieri C, Valdemarin F, Becherini P, Wei M, et al. Fasting-mimicking diet and hormone therapy induce breast cancer regression. Nature. 2020;583:620–4.
4. Dmitrieva-Posocco O, Wong AC, Lundgren P, Golos AM, Descamps HC, Dohnalová L, et al. β-Hydroxybutyrate suppresses colorectal cancer. Nature. 2022;605:160–5.

5. Solanki S, Sanchez K, Ponnusamy V, Kota V, Bell HN, Cho CS, et al. Dysregulated amino acid sensing drives colorectal cancer growth and metabolic reprogramming leading to chemoresistance. Gastroenterology. 2023;164:376–391.e313.
6. Lee C, Raffaghello L, Brandhorst S, Safdie FM, Bianchi G, Martin-Montalvo A, et al. Fasting cycles retard growth of tumors and sensitize a range of cancer cell types to chemotherapy. Sci Transl Med. 2012;4:124ra127.
7. Cortellino S, Raveane A, Chiodoni C, Delfanti G, Pisati F, Spagnolo V, et al. Fasting renders immunotherapy effective against low-immunogenic breast cancer while reducing side effects. Cell Rep. 2022;40:111256.
8. Vernieri C, Fucà G, Ligorio F, Huber V, Vingiani A, Iannelli F, et al. Fasting-mimicking diet is safe and reshapes metabolism and antitumor immunity in patients with cancer. Cancer Discov. 2022;12:90–107.
9. Di Biase S, Lee C, Brandhorst S, Manes B, Buono R, Cheng CW, et al. Fasting-mimicking diet reduces HO-1 to promote T cell-mediated tumor cytotoxicity. Cancer Cell. 2016;30:136–46.
10. Janssen H, Kahles F, Liu D, Downey J, Koekkoek LL, Roudko V, et al. Monocytes re-enter the bone marrow during fasting and alter the host response to infection. Immunity. 2023;56:783–796.e787.
11. Clifton KK, Ma CX, Fontana L, Peterson LL. Intermittent fasting in the prevention and treatment of cancer. CA Cancer J Clin. 2021;71:527–46.
12. Salvadori G, Zanardi F, Iannelli F, Lobefaro R, Vernieri C, Longo VD. Fasting-mimicking diet blocks triple-negative breast cancer and cancer stem cell escape. Cell Metab. 2021;33:2247–259.e2246.
13. Pietrocola F, Pol J, Vacchelli E, Rao S, Enot DP, Baracco EE, et al. Caloric restriction mimetics enhance anticancer immunosurveillance. Cancer Cell. 2016;30:147–60.
14. Christofides A, Strauss L, Yeo A, Cao C, Charest A, Boussiotis VA. The complex role of tumor-infiltrating macrophages. Nat Immunol. 2022;23:1148–56.
15. Cheng K, Cai N, Zhu J, Yang X, Liang H, Zhang W. Tumor-associated macrophages in liver cancer: from mechanisms to therapy. Cancer Commun (Lond). 2022;42:1112–40.
16. Vogel A, Meyer T, Sapisochin G, Salem R, Saborowski A. Hepatocellular carcinoma. Lancet. 2022;400:1345–62.
17. Safdie F, Brandhorst S, Wei M, Wang W, Lee C, Hwang S, et al. Fasting enhances the response of glioma to chemo- and radiotherapy. PLoS One. 2012;7:e44603.
18. Lo Re O, Panebianco C, Porto S, Cervi C, Rappa F, Di Biase S, et al. Fasting inhibits hepatic stellate cells activation and potentiates anti-cancer activity of Sorafenib in hepatocellular cancer cells. J Cell Physiol. 2018;233:1202–12.
19. Krstic J, Reinisch I, Schindlmaier K, Galhuber M, Riahi Z, Berger N, et al. Fasting improves therapeutic response in hepatocellular carcinoma through p53-dependent metabolic synergism. Sci Adv. 2022;8:eabh2635.
20. Sangro B, Sarobe P, Hervás-Stubbs S, Melero I. Advances in immunotherapy for hepatocellular carcinoma. Nat Rev Gastroenterol Hepatol. 2021;18:525–43.
21. Llovet JM, Castet F, Heikenwalder M, Maini MK, Mazzaferro V, Pinato DJ, et al. Immunotherapies for hepatocellular carcinoma. Nat Rev Clin Oncol. 2022;19:151–72.
22. Chen J, Lin Z, Liu L, Zhang R, Geng Y, Fan M, et al. GOLM1 exacerbates CD8(+) T cell suppression in hepatocellular carcinoma by promoting exosomal PD-L1 transport into tumor-associated macrophages. Signal Transduct Target Ther. 2021;6:397.
23. Lu LG, Zhou ZL, Wang XY, Liu BY, Lu JY, Liu S, et al. PD-L1 blockade liberates intrinsic antitumourigenic properties of glycolytic macrophages in hepatocellular carcinoma. Gut. 2022;71:2551–60.
24. Zhang H, Liu L, Liu J, Dang P, Hu S, Yuan W, et al. Roles of tumor-associated macrophages in anti-PD-1/PD-L1 immunotherapy for solid cancers. Mol Cancer. 2023;22:58.
25. Noguchi T, Ward JP, Gubin MM, Arthur CD, Lee SH, Hundal J, et al. Temporally distinct PD-L1 expression by tumor and host cells contributes to immune escape. Cancer Immunol Res. 2017;5:106–17.
26. Tang H, Liang Y, Anders RA, Taube JM, Qiu X, Mulgaonkar A, et al. PD-L1 on host cells is essential for PD-L1 blockade-mediated tumor regression. J Clin Invest. 2018;128:580–8.
27. Lin H, Wei S, Hurt EM, Green MD, Zhao L, Vatan L, et al. Host expression of PD-L1 determines efficacy of PD-L1 pathway blockade-mediated tumor regression. J Clin Invest. 2018;128:805–15.
28. Niu M, Liu Y, Yi M, Jiao D, Wu K. Biological characteristics and clinical significance of soluble PD-1/PD-L1 and exosomal PD-L1 in cancer. Front Immunol. 2022;13:827921.
29. Fan Y, Che X, Qu J, Hou K, Wen T, Li Z, et al. Exosomal PD-L1 retains immunosuppressive activity and is associated with gastric cancer prognosis. Ann Surg Oncol. 2019;26:3745–55.
30. Poggio M, Hu T, Pai CC, Chu B, Belair CD, Chang A, et al. Suppression of exosomal PD-L1 induces systemic anti-tumor immunity and memory. Cell. 2019;177:414–427.e413.
31. Cai N, Cheng K, Ma Y, Liu S, Tao R, Li Y, et al. Targeting MMP9 in CTNNB1 mutant hepatocellular carcinoma restores CD8(+) T cell-mediated antitumour immunity and improves anti-PD-1 efficacy. Gut. 2024;73:985–99.
32. Brandhorst S, Longo VD. Dietary restrictions and nutrition in the prevention and treatment of cardiovascular disease. Circ Res. 2019;124:952–65.
33. Ma S, Sun B, Duan S, Han J, Barr T, Zhang J, et al. YTHDF2 orchestrates tumor-associated macrophage reprogramming and controls antitumor immunity through CD8(+) T cells. Nat Immunol. 2023;24:255–66.
34. Zhong W, Lu Y, Han X, Yang J, Qin Z, Zhang W, et al. Upregulation of exosome secretion from tumor-associated macrophages plays a key role in the suppression of anti-tumor immunity. Cell Rep. 2023;42:113224.
35. Pan T, Zhou Q, Miao K, Zhang L, Wu G, Yu J, et al. Suppressing Sart1 to modulate macrophage polarization by siRNA-loaded liposomes: a promising therapeutic strategy for pulmonary fibrosis. Theranostics. 2021;11:1192–206.
36. Wang Z, Li M, Jiang H, Luo S, Shao F, Xia Y, et al. Fructose-1,6-bisphosphatase 1 functions as a protein phosphatase to dephosphorylate histone H3 and suppresses PPARα-regulated gene transcription and tumour growth. Nat Cell Biol. 2022;24:1655–65.
37. Kimura S, Khalil IA, Elewa YHA, Harashima H. Novel lipid combination for delivery of plasmid DNA to immune cells in the spleen. J Control Release. 2021;330:753–64.
38. Mao YQ, Huang JT, Zhang SL, Kong C, Li ZM, Jing H, et al. The antitumour effects of caloric restriction are mediated by the gut microbiome. Nat Metab. 2023;5:96–110.
39. Montégut L, de Cabo R, Zitvogel L, Kroemer G. Science-driven nutritional interventions for the prevention and treatment of cancer. Cancer Discov. 2022;12:2258–79.
40. de Groot S, Lugtenberg RT, Cohen D, Welters MJP, Ehsan I, Vreeswijk MPG, et al. Fasting mimicking diet as an adjunct to neoadjuvant chemotherapy for breast cancer in the multicentre randomized phase 2 DIRECT trial. Nat Commun. 2020;11:3083.
41. Collins N, Han SJ, Enamorado M, Link VM, Huang B, Moseman EA, et al. The bone marrow protects and optimizes

immunological memory during dietary restriction. Cell. 2019;178:1088–1101.e1015.
42. Chen G, Huang AC, Zhang W, Zhang G, Wu M, Xu W, et al. Exosomal PD-L1 contributes to immunosuppression and is associated with anti-PD-1 response. Nature. 2018;560:382–6.
43. Weng ML, Chen WK, Chen XY, Lu H, Sun ZR, Yu Q, et al. Fasting inhibits aerobic glycolysis and proliferation in colorectal cancer via the Fdft1-mediated AKT/mTOR/HIF1α pathway suppression. Nat Commun. 2020;11:1869.

How to cite this article: Cheng K, Cai N, Yang X, Li D, Jinghan Z, Yang HY, et al. Short-term starvation boosts anti-PD-L1 therapy by reshaping tumor-associated macrophages in hepatocellular carcinoma. Hepatology. 2025;82:1414–1431. https://doi.org/10.1097/HEP.0000000000001244